A woolly mammoth (Mammuthus primigenius) carcass from Maly Lyakhovsky Island (New Siberian Islands, Russian Federation)

Grigoriev, Semyon E.; Fisher, Daniel C.; Obada, Theodor; Shirley, Ethan A.; Rountrey, Adam N.; Savvinov, Grigory N.; Garmaeva, Darima K.; Novgorodov, Gavril P.; Cheprasov, Maksim Yu.; Vasilev, Sergei E.

Published in:
Quaternary International

DOI:
10.1016/j.quaint.2017.01.007

Publication date:
2017

Quaternary International 445 (2017) 89–103

Contents lists available at ScienceDirect

Quaternary International

journal homepage: www.elsevier.com/locate/quaint

A woolly mammoth (*Mammuthus primigenius*) carcass from Maly Lyakhovsky Island (New Siberian Islands, Russian Federation)

Semyon E. Grigoriev [a, **], Daniel C. Fisher [b, *], Theodor Obadă [c], Ethan A. Shirley [b], Adam N. Rountrey [b], Grigory N. Savvinov [d], Darima K. Garmaeva [e], Gavril P. Novgorodov [a], Maksim Yu. Cheprasov [a], Sergei E. Vasilev [f], Artemiy E. Goncharov [g, h, i], Alexey Masharskiy [i], Viktoriya E. Egorova [e], Palmira P. Petrova [e], Eya E. Egorova [e], Yana A. Akhremenko [e], Johannes van der Plicht [j], Alexei A. Galanin [k], Sergei E. Fedorov [a], Evgeny V. Ivanov [d], Alexei N. Tikhonov [l, a, ***]

[a] *Lazarev Mammoth Museum, Institute of Applied Ecology of the North, North-Eastern Federal University, Yakutsk, Russian Federation*
[b] *Museum of Paleontology, University of Michigan, Ann Arbor, MI, USA*
[c] *Institute of Zoology, Academy of Sciences of Moldova, Chişinău, Republic of Moldova*
[d] *Institute of Applied Ecology of the North, North-Eastern Federal University, Yakutsk, Russian Federation*
[e] *Medical Institute, North-Eastern Federal University, Yakutsk, Russian Federation*
[f] *3D Modelling and Virtual Reality Center, Institute of Physics and Technologies, North-Eastern Federal University, Yakutsk, Russian Federation*
[g] *North-West State Medical University named after I.I. Mechnikov, Saint-Petersburg, Russian Federation*
[h] *Institute of Experimental Medicine, Saint-Petersburg, Russian Federation*
[i] *Saint Petersburg State University, Saint-Petersburg, Russian Federation*
[j] *Center for Isotope Research, Groningen University, Groningen, The Netherlands*
[k] *Melnikov Permafrost Institute, Siberian Branch of the Russian Academy of Sciences, Yakutsk, Russian Federation*
[l] *Zoological Institute, Russian Academy of Sciences, Saint-Petersburg, Russian Federation*

ARTICLE INFO

Article history:
Received 1 March 2016
Received in revised form
2 December 2016
Accepted 9 January 2017
Available online 1 March 2017

Keywords:
Mammuthus primigenius
Maly Lyakhovsky Island
Late Pleistocene
Life history
Soft tissue preservation
Permafrost

ABSTRACT

A partial carcass of an adult woolly mammoth (*Mammuthus primigenius*) found in 2012 on Maly Lyakhovsky Island presents a new opportunity to retrieve associated anatomical, morphological, and life history data on this important component of Pleistocene biotas. In addition, we address hematological, histological, and microbiological issues that relate directly to quality of preservation. Recovered by staff from North-Eastern Federal University in Yakutsk, this individual is a relatively old female preserving soft tissue of the anteroventral portion of the head, most of both fore-quarters, and the ventral aspect of much of the rest of the body. Both tusks were recovered and subjected to computed tomographic analysis in which annual dentin increments were revealed as cycles of variation in X-ray attenuation. Measurements of annual increment areas (in longitudinal section) display a pulsed pattern of tusk growth showing cycles of growth rate variation over periods of 3–5 years. These intervals are interpreted as calving cycles reflecting regular shifts in calcium and phosphate demand for tusk growth vs. fetal ossification and lactation. Brown liquid associated with the frozen carcass turned out to include remains of hemolyzed blood, and blood samples examined microscopically included white blood cells with preserved nuclei. Muscle tissue from the trunk was unusually well preserved, even at the histological level. Intestinal contents and tissue samples were investigated microbiologically, and several strains of lactic-acid bacteria (e.g., *Enterococcus faecium, Enterococcus hirae*) that are widely distributed as commensal organisms in the intestines of herbivores were isolated.

1. Introduction

In mid-August, 2012, commercial ivory prospectors hunting for mammoth tusks discovered a partial carcass of an adult woolly

* Corresponding author.
** Corresponding author.
*** Corresponding author. Zoological Institute, Russian Academy of Sciences, Saint-Petersburg, Russian Federation.
E-mail addresses: g_semen@mail.ru (S.E. Grigoriev), dcfisher@umich.edu (D.C. Fisher), atikh@mail.ru (A.N. Tikhonov).

http://dx.doi.org/10.1016/j.quaint.2017.01.007
1040-6182/

mammoth (*Mammuthus primigenius*) on Maly Lyakhovsky Island. This island is one of the New Siberian Islands, located between the Laptev Sea and the East Siberian Sea (Fig. 1). The remains were found 200 m from the northeast coast of the island, on a low hill. Material that was exposed at the time of discovery included various post-cranial elements, skull fragments, and the mammoth's trunk, which lay across the left tusk.

Recognizing the possible significance of this find, the ivory prospectors recorded its location, notified staff of the Lazarev Mammoth Museum (Institute of Applied Ecology of the North, North-Eastern Federal University, Yakutsk), and agreed to retain, rather than immediately sell, the relatively small tusks they had found with this specimen. During the following months, staff of the Museum and Institute devised a plan to return to the discovery site and extract the specimen.

The goal of this article is to summarize some of the first results of analyses of this specimen. Most other recent discoveries of mammoth specimens with preserved soft tissue have been juveniles (e.g., Shilo et al., 1983; Boeskorov et al., 2007a; Fisher et al., 2012; Kosintsev et al., 2012; Maschenko et al., 2013; Boeskorov et al., 2014) or adolescents (Pitulko et al., 2016), with a smaller number of adult males (e.g., Mol et al., 2001; Boeskorov et al., 2007b). The prospect of retrieving data from another adult, especially if it might turn out to be an adult female, was a strong attraction. The focus of our morphological and anatomical studies is on issues related to sex, life history, and preservation. In relation to the latter point, we especially sought to clarify the nature of a brown liquid discovered in close association with the carcass at the time of its excavation. Its appearance was suggestive of blood, but entertaining such an idea required us to assess preservation at a variety of levels. In addition to hematological analysis, we evaluated preservation of cell and tissue structures in the first histological examination of this specimen. Finally, we cultured and sequenced numerous microbial taxa from tissues and intestinal contents. Comprehensive description of this specimen is beyond the scope of this paper, but we hope to provide a foundation for a wide range of subsequent studies.

2. Material

2.1. Specimen recovery

Staff from the Museum and Institute departed from Yakutsk on 29 April 2013 and traveled by plane and car to the settlement of Kazachie (Ust'-Yanskiy district). Knowing that significant amounts of soft tissue from this mammoth had been exposed at the surface, and that more probably remained within the permafrost, they planned to execute the recovery under conditions that would remain consistently below freezing, while avoiding the extreme cold of mid-winter. Moreover, it would be necessary not only to reach the discovery site and extract the specimen, but also to return it to the mainland.

A team of three staff from the Museum and Institute, assisted by members of the team of ivory prospectors who had discovered the specimen, set out from Kazachie on snowmobiles pulling sleds loaded with supplies and equipment on 5 May 2013. Normal conditions for this region, at this time of year, would have been well below freezing, but with each year now bringing an earlier end to

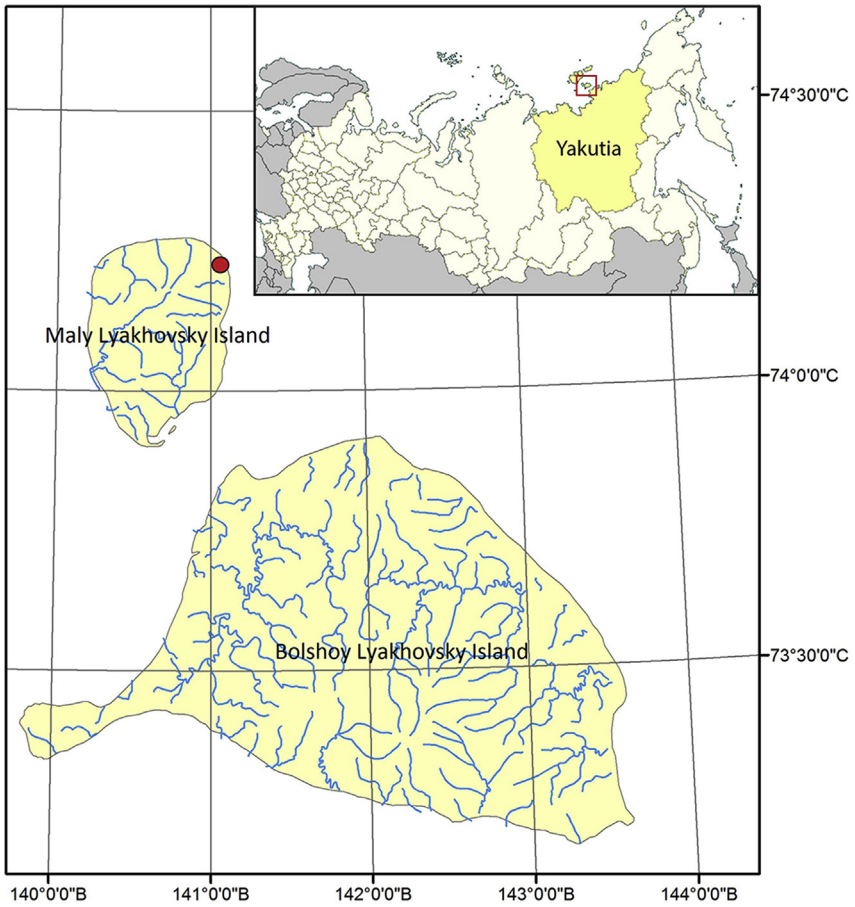

Fig. 1. Geographical position of Maly Lyakhovsky Island, north of the Arctic coast of Yakutia (yellow region on map inset; light gray in print version), in the northeastern portion of the Russian Federation. (For interpretation of the references to colour in this figure legend, the reader is referred to the web version of this article.)

winter, the tundra surface around Kazachie was already melting extensively. The recovery party crossed the ice-covered Dmitry Laptev Strait, where rapidly changing weather and sea-ice conditions presented grave dangers, continued overland across Bolshoy Lyakhovsky Island, and then crossed more sea-ice to Maly Lyakhovsky Island.

Arriving at the site on 9 May, the recovery party began excavating the mammoth using hand tools and a pneumatic jackhammer to chip away ice and frozen sediment. In parallel, they collected all skeletal elements that could be found at the surface, but remaining snow made it likely that some were overlooked. Following the specimen downward into the permafrost, the excavators had to reassess constantly what could be identified as it was exposed and what could be inferred to have been exposed already, based on material recovered from the surface. In this fashion, the team deduced that only the lower half of the mammoth carcass remained intact and that the specimen was more complete anteriorly than posteriorly (Fig. 2). Although normal permafrost was present in the immediate vicinity of the specimen, most of the body turned out to be directly surrounded by clean ice rather than frozen sediment, indicating that the body must have been immersed in water such as might collect in a small pond or depression on the tundra surface. To recover the carcass in the best possible condition, the team decided to leave some ice intact surrounding the original skin surface. On the other hand, to remove the specimen by hand and load it onto the sturdiest of the sleds, it was important to reduce its mass as much as possible, eventually to about 350 kg.

While working in the right axillary region and below the venter, the team encountered ice cavities holding small amounts of dark brown liquid, 3 ml of which were transferred to two sample tubes. Ambient temperature at this time was no more than −5 °C, and yet this liquid remained unfrozen, prompting speculation as to what aspect of its composition permitted it to remain free-flowing under these conditions. In addition, the color of this liquid raised the question of whether it might somehow, or to some degree, represent blood of the mammoth. While in the field, little could be determined with certainty, but clarifying the nature of this liquid became a prime objective.

Working around the specimen gradually, the team eventually isolated it and loaded it onto a steel sledge. As a precaution against damage on the journey back to the south, snow was packed around exposed parts of the carcass, and water was poured over this and allowed to freeze, forming a protective layer. The entire mass was then wrapped in a plastic tarp and lashed to the sledge. As soon as possible, the team set out over the rapidly deteriorating sea-ice and successfully regained the security of the mainland. Once back in Kazachie, they stored the specimen in a community-managed “ice-cave” (lyednik; used normally for food storage) that had been dug into the permafrost.

2.2. Specimen examination

In August, 2013 an international group of scientists (some of the authors of this article and the South Korean biotechnology research group SOOAM) assembled in Kazachie to begin more detailed evaluation of the mammoth. While the carcass was still fully frozen, we cut through the protective layer of ice and snow and removed blocks of frozen soft tissue from the legs and flank of the animal, providing samples that had not been thawed, at least in recent times. The carcass, still on its sledge, was then pulled out of the ice-cave so that it could be examined in daylight. Exterior temperatures at that time were on the order of 5–10 °C, and yet the thermal inertia of the specimen was great enough that most of the larger masses (such as the limbs) did not completely thaw during the three-day period allowed for this phase of the study.

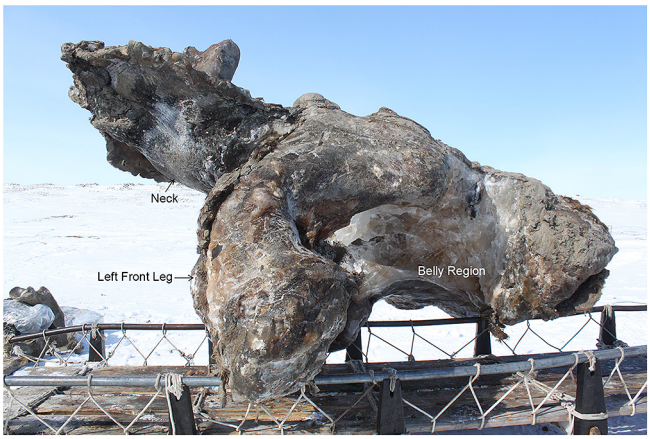

Fig. 2. Left lateral view of articulated mammoth remains on sledge after excavation; anterior toward upper left.

The next step was to carefully chip away the protective layer of frozen snow and ice, or in some cases, simply allow it to melt. Additional sampling of soft tissues just as they were exposed, yet before melting, occurred at this point. Parts of the body revealed in this fashion were covered by skin, except where the active layer of the permafrost – the near-surface zone of seasonal melting (and degradation of constituent organic materials) – had truncated the carcass along a roughly planar surface that angled from the mammoth's forehead, downward and backward through the neck, intersecting the thorax and abdomen below the axial skeleton and pelvis. Below this plane, the lower part of the head, the distal portion of the trunk, the lower neck, chest, and belly, the front legs, and the distal half of the right hind leg remained in excellent condition.

While exposing and examining intact parts of the carcass (described more fully under Results), disarticulated material that had been recovered from the ground surface around the carcass was also reviewed and identified. In contrast to body parts that had remained below the active layer of the permafrost, most soft tissues on the rest of the body had decomposed, leaving bones with little more than shreds of connective tissue and degraded masses of fat and adipocere. Some of these bones showed clear evidence of gnawing by predators and/or scavengers. Some of this modification could have occurred in close conjunction with the death of this animal, but some could also have been due to recent activity following exhumation of the specimen by normal processes of melting and erosion of permafrost.

Following this initial examination and sampling, the remaining intact part of the carcass (now reduced to about 135 kg) and all disarticulated elements were returned to the sub-freezing conditions of the ice-cave (ca. −10 °C) and left there until the following winter. In February, 2014, the entire specimen was loaded onto a truck and transported south to Yakutsk, where it was stored in an above-ground, urban equivalent of an ice-cave. During the week of 10–14 March, it was subjected to a second round of partial thawing, examination, and sampling by another international group of investigators. At the end of this week, the specimen was returned to freezing conditions, where it remains currently. The laboratory analyses discussed below were designed to address issues raised by these first examinations and take advantage of opportunities presented by this specimen.

3. Methods

Methods applied in this study are described in Supplemental

material section S1.

4. Results

4.1. General anatomy and preservation

The part of the mammoth that was encountered first and that seems to have best retained its external appearance is the trunk, or proboscis. At its distal end is the single anterior projection opposed by two posterior lobes that collectively form the grasping tip of this remarkable appendage (Fig. 3A). The general form of this tip matches that of previously recovered specimens, but other specimens were all more strongly desiccated or otherwise degraded. Only the Malolyakhovsky trunk tip approximates the likely appearance of this structure in the living animal, with its normal level of tissue hydration. Unlike most forelimb muscle tissue, which was brownish in color, some muscles of the trunk were preserved well enough to retain their natural red color (Fig. 3B).

Three fragments of trunk tissue were collected at the site, the first of which was a 90-cm fragment that was cut away from the carcass by the tusk prospectors. After cleaning (during the examinations in Kazachie and Yakutsk), it was possible to refit the pieces relatively precisely, yielding a single assembly 181 cm long, measuring with a flexible tape measure around the curved tip, along the dorsal surface, to the proximal-most extent of the skin (Fig. 3C). Some skin is missing from the proximal part of the proboscis, where it would have extended across the forehead, but the measured length is at least generally representative.

As soon as the distal part of the trunk was removed, the tusks were collected by the tusk hunters and later secured in a private ice-cave in Kazachie. Their gross dimensions are reported here, and they are illustrated in Fig. 4, but additional details are provided in subsequent sections. The right tusk weighs 17.6 kg and is 207.5 cm long measured along its outside curve, with a basal circumference of 28.6 cm and a circumference of 27.9 cm at mid-length. Its pulp cavity depth is 11.9 cm. The left tusk weighs 16.6 kg and is 223 cm long on its outside curve, with a basal circumference of 25.4 cm and a circumference of 27.5 cm at mid-length. Its pulp cavity depth is 11.5 cm. Circumference profiles (variation in circumference with distance from distal end) are provided in Table S1 in Supplemental material.

The maxillae were also exposed at the surface, in close conjunction with the premaxillae and tusks. In fact, the maxillae were probably removed from the premaxillae during removal of the tusks. As part of this process, the maxillae were also detached from associated soft tissue, although the premaxillae (with their lateral alveolar walls broken away to release the tusks) retained a soft-tissue connection. The dentaries remained deeply embedded within soft tissues of the oral region, but during the examination in Kazachie, it became clear that the mandible had been broken just to the left of the symphysis. We do not know when this break occurred, but it must have been before collection. During the necropsy in Yakutsk, the dentaries and premaxillae were separated from associated soft tissue, and after this, the fracture near the mandibular symphysis was repaired. The elements bearing the cheek-tooth dentition are illustrated in Fig. 5 by post-necropsy photos.

The upper molars are deeply worn, with anterior plates worn to the roots (measurements in Table 1). Both are abnormally curved (concave toward the midline). Curvature of the left is more extreme and involves strong accentuation of what is normally only a subtle curvature of the long axis of the tooth, such that the posterior lamellae are rotated at least 60° clockwise, looking at the occlusal surface from below (Fig. 5). Curvature of the right is less severe, with the main tooth axis being much more normal. However, on this tooth, the impression of curvature is more a function of rotation of anterior lamellae, especially those now worn off to the roots. It is further accentuated by an indentation along the lingual margin of the tooth at a position about half-way along the length of the remaining part of the crown. This indentation is not due to a process such as resorption operating on the mature crown. Rather, it represents a developmental anomaly in which lamellae 7–9 (counting from the front of the tooth) do not extend lingually as far as would be expected. The advanced wear at the front of each tooth means that our length measurements and plate numbers are only minimum values, and the curvature of the teeth makes width measurements suspect. Taking measurements of these teeth at face value, and comparing with published reports (e.g., Maglio, 1973), it would be impossible to distinguish whether we were dealing with M2s or M3s. That is, these teeth are small enough to be interpreted either as M2s somewhat reduced by attrition or M3s greatly reduced by attrition. We return to this issue below and in the Discussion section.

In contrast to the uppers, both lower teeth show more nearly normal crown configurations and measurements that are most compatible with interpreting them as m3s (Table 1). We know that these have lost lamellae (and crown length) anteriorly as well, in part because one or more of the anterior roots has been undercut and removed. Posteriorly, each of these teeth also shows a tapered terminus characteristic of many third molars (Lister and Sher, 2015). Given this interpretation of the lowers, it seems most parsimonious to interpret the uppers as M3s as well, but we return to this in the Discussion. The wear stage of the left m3 matches Laws' (1966) age group XXV (the right is slightly more advanced), suggesting an age of about 47 yr (refined further in the Discussion section).

When the carcass emerged from the ice-cave in Kazachie, all of the skin from the lower part of the head was frozen into a solid block, but as this began to thaw, we were slowly able to work individual structures free from this mass and recognize their anatomical relations. We were eventually able to explore the entire oral cavity, but there was no trace of the tongue. However, we did find the gingival margins of the maxillary and mandibular dentition, where the oral mucosa and underlying tissue had been removed from the bone.

Most impressive was the elasticity of the skin around the mouth, but its morphology was also notable. At the median, anteroventral position along the oral margin was a pointed, down-turned spout-like protrusion that must have overlain the mandibular symphysis. Following the acute margins of the lower lips backward, the space between them widened (Fig. 6A). Approaching the posterior-most “corners” of the mouth, the margin of the lower lip transitioned into a zone of multiple transverse folds that accommodated an unexpectedly wide gape when the mouth was stretched open, and yet these folds retracted back to form a compact transition to the upper lip when the mouth was closed again. The upper lips were much broader (in the lingual-buccal direction) than the lower lips, and their thicker margins hung down lateral to the acute margins of the lower lips when the mouth was closed. Especially prominent were large, lobate projections from the anterolateral portions of the upper lips. These slid into positions lateral to the posterior parts of the upper lips when the mouth was closed and yet rotated forward to extend the anterolateral margin of the oral cavity when the mouth opened.

Anteriorly, the lobate extensions of the upper lips would have been closely adherent to the gingival margin on the lateral aspects of the tusks. The tusks had already been removed from their alveoli prior to our examination of the carcass in Kazachie, but part of the gingival margin of the left tusk can be seen near the upper right margin of Fig. 6A (*gm*), where the left lobate lip margin has slumped

Fig. 3. Proboscis of the Malolyakhovsky mammoth. **A.** Distal part of trunk (with 5-cm scale) following partial cleaning by rinsing with fresh water (rounded tip of trunk was cut off by a South Korean researcher shortly before this photo was taken. B. Incision showing well-preserved (red; near scalpel, but only distinguishable in online color version) trunk muscle tissue. C. Three pieces of the trunk recovered from the site and reassembled; dorsal length measured with a flexible tape along the curve was 181 cm (scale bar is 20 cm). (For interpretation of the references to colour in this figure legend, the reader is referred to the web version of this article.)

laterally. One anomaly that puzzled us at the time of our first examination was the breadth of the anteromedian portion of the upper lip (underneath the gloved hand in Fig. 6A). In *M. primigenius*, the tusks are usually close to each other (and to the midline) where they exit from the premaxillae at their medial alveolar margins. Yet the configuration of this soft tissue implies that the tusks were ca. 15 cm from one another at their alveolar margin. On the other hand, judging from the soft tissue of the palatal region, the gingival

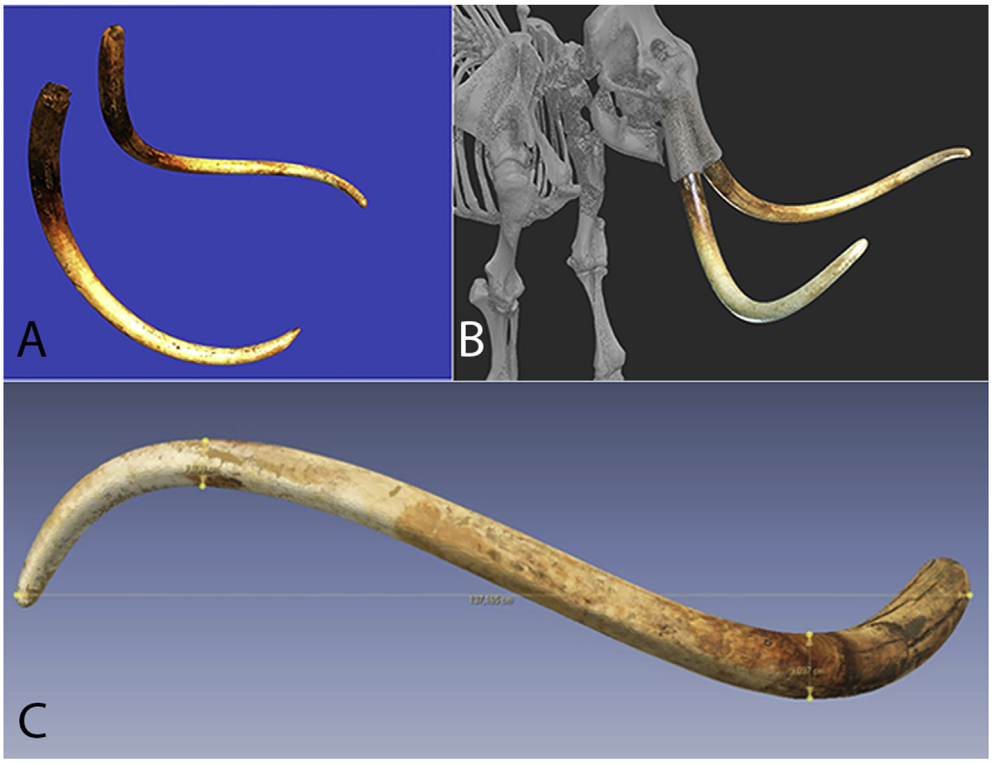

Fig. 4. Tusks of the Malolyakhovsky mammoth. A. Texture-mapped 3D models of the left and right tusks of the Malolyakhovsky mammoth, in an approximately dorsolateral view. B. Both tusks inserted in the 3D mammoth model from the Smithsonian Institution (http://3d.si.edu/). C. Close-up of texture-mapped 3D model of left tusk showing measurements (faint yellow end-point markers and lines, white in print version; numeric data not legible at this scale) of chord-length and diameters at two positions. Darkly pigmented ring just proximal to the right-most diameter measurement marks the approximate location of the alveolar margin; the gingival margin is just distal to this. (For interpretation of the references to colour in this figure legend, the reader is referred to the web version of this article.)

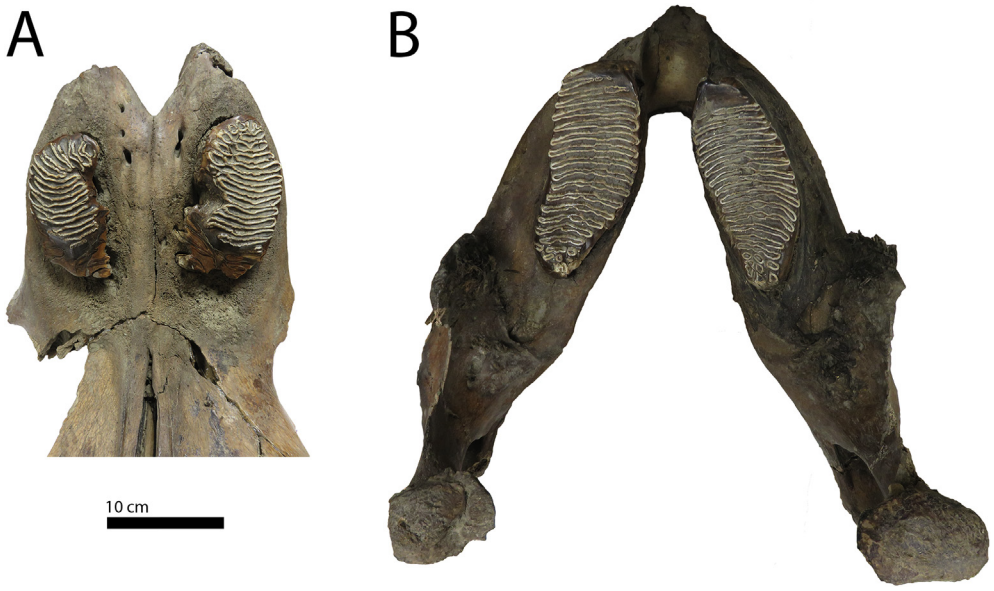

Fig. 5. Maxillary and mandibular dentition of Malolyakhovsky mammoth. A. Occlusal view of maxillae with upper teeth (and part of premaxillae below; anterior toward bottom; left upper tooth on left; right upper tooth on right). Scale bar is 10 cm long. B. Occlusal view of mandible with lower teeth (anterior toward top; left lower tooth on left; right lower tooth on right). Scale as for A.

margins for the tusks seem too close to the location of the upper molars (inferred from the location of the openings in the palatal mucosa). We were finally able to resolve this issue when we compared the soft tissue with the underlying bone from which it had been removed (Supplemental material, Fig. S1). The anterior breadth of the left and right premaxillae (12.3 cm) is indeed consistent with the medial spacing between the tusks at their gingival margins, but the anteroventral end of the premaxillae is 47 cm below and in front of the anterior margins of the upper molars, much farther than we would have judged from the soft tissue. This means that the soft tissue must have been stretched tightly over the bone, especially in the longitudinal direction, and subsequently contracted following removal.

Other impressive examples of soft tissue preservation are the breasts and nipples of the mammoth. The right breast, with its conical nipple, is shown in Fig. 6B, just as it was melting out of the ice covering the ventral aspect of the animal. The left breast was similar in profile, but its nipple was more cylindrical and longer. This nipple appeared to have sustained slight damage distally, possibly during excavation; on its damaged terminus opened several patent milk ducts.

Both forelimbs were articulated and in primary anatomical association with the ventral portion of the head, neck, and chest, all with preserved soft tissue. The left forelimb was flexed about 90° at the elbow and wrist (Fig. S2), and the right forelimb was flexed even more (Fig. S3). The lower right hind limb was the only part of a rear leg that remained fully articulated and encased in soft tissue. It was located below the posterior-most part of the venter and was oriented transversely, with the tibia and fibula horizontal and the sole of the right foot facing toward the left (right margin of Fig. S2). Its position suggested the possibility of a remnant anatomical association with the back end of the body, but there was no actual connection via the right thigh or pelvic girdle.

Foot and limb dimensions have been used in various ways to estimate proboscidean stature. In our case, associated soft tissues made it difficult to measure shoulder height either directly or via CT methods. However, Sukumar et al. (1988) showed that for Asian elephants (*Elephas maximus*), shoulder height is approximately 2.03 times front foot circumference. The left front foot of our specimen (anteroposterior length 36.5 cm; transverse breadth 36.8 cm) has a circumference of 118 cm, and we therefore estimate a shoulder height of 240 cm.

The hair of this mammoth was variable in length, but none of it was more than 50 cm long, and most was less than 20 cm long. Hair on the trunk was relatively sparse, with little underwool. Underwool was present on other parts of the body, but it was less dense than we have observed on other specimens. Most of the hair we observed was encased in relatively clear ice. In several places, the ice also contained remains of green plants, and the hair and surrounding ice were in places stained reddish-brown, which was suggestive of blood and reminiscent of the dark brown liquid recovered during excavation. Underneath and beside the carcass, in

Table 1
Measurements of the last molars (M3 and m3) of *Mammuthus primigenius* from Maly Lyakhovsky Island (following Garutt and Foronova, 1976).

Molar/Measurement	M3 dexter	M3 sinister	m3 sinister	m3 dexter
Tooth crown wear stage	6	6	5–6	5–6
Number of enamel plates	>13	>15	>19	>20
Length (mm)	>129	>131	200	197
Width (mm)	69.7 (6)	63.2 (7)	71.5 (8)	69.7 (9)
Height (mm)	>21	>25	>36	>32
Length of one plate (mm)	8.8	10.4	10.8	10.5
Plate frequency (per 10 cm)	10.5	10.5	8.6	9.7
Enamel thickness (mm)	2.00	1.97	1.97	2.03

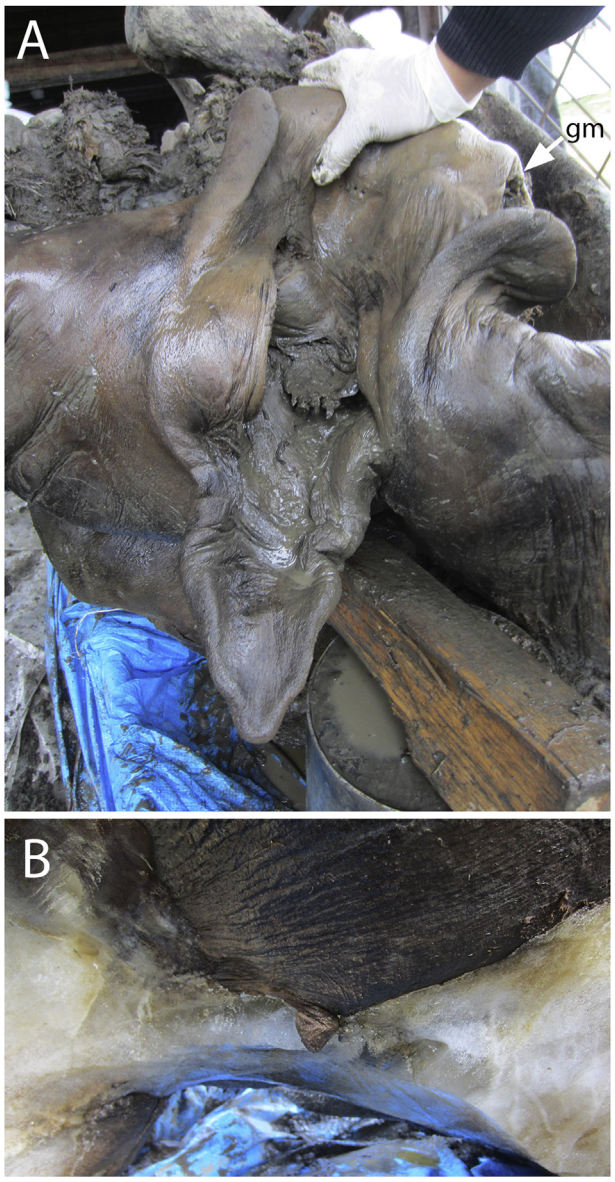

Fig. 6. Soft-tissue features of the Malolyakhovsky mammoth. A. Anterior aspect of oral region, with gloved hand at top pushing upper lip up and back to hold mouth in an open position. The pointed lower lip is directed forward and downward at the mid-line position along the margin of the oral cavity. Lobate projections from lateral margins of upper lip can be seen below and on each side of the gloved hand. Arrow labeled *gm* indicates the gingival margin of the left tusk. Blue tarp (online color version) in lower part of image had been wrapped around the carcass for protection during transport. A piece of wood lying across the bottom of a bucket holds the "chin" in position. B. Medial aspect of right breast, just melting free of surrounding ice. Nipple is located centrally and is about 2 cm in diameter at its base. (For interpretation of the references to colour in this figure legend, the reader is referred to the web version of this article.)

ice, we found several chunks of muscle tissue and one fragment of rib with associated muscle tissue, skin, hair, and blood.

Most of the contents of the pleural and visceral cavities had been disrupted dorsally by some combination of erosion, weathering, predation, and scavenging. We did, however, find tissues that were readily associated with particular structures or organs, based on their location, their structure, and gross characteristics of their tissue. In this fashion, we recognized fragments of liver, stomach, intestines, pericardium, and diaphragm. From the intestines, we recovered partly digested plant remains, samples of which were used for microbiological studies described below.

While investigating the visceral cavity by excavating downward through the zone of decomposition that followed the Recent land surface and truncated the thorax, we noticed evidence of a large hematoma on the lateral wall of the abdomen, within muscle tissue between the lower portions of two ribs on the right side. An incision into this feature revealed a large volume of coagulated blood, encased within surrounding tissue (Figs. S4-S6). This feature is a clear indication of perimortem trauma.

Many dorsal and posterior parts of the body – the skull (broken into several pieces), axial skeleton, dorsal parts of ribs, the right innominate, the right femur, and the left hind leg – were recovered from the surface of the tundra near the articulated part of the carcass and were represented mainly by separate bones, most of which were gnawed to various degrees by predators or scavengers. Despite our best efforts, only a few vertebrae and about half of the ribs were recovered during the excavation and examination of the surrounding surface of the site. The left innominate was not recovered, but most of the left hind limb (femur through pes) was recovered in approximate anatomical association, stretched out behind the rest of the body, with wool and fat around the knee and foot. In Supplemental material, Tables S2-S5 provide representative measurements of some postcranial elements. Throughout the skeleton, epiphyses and diaphyses were completely fused.

4.2. Radiocarbon dating

The results of AMS dating and carbon and nitrogen isotope and elemental analyses are shown in Table 2. The ^{14}C dates for both samples show excellent agreement. Their averaged value is 28,610 ± 110 BP. The calibrated age range for this date (obtained using IntCal13) is 32,930–32,480 cal BP (1-sigma).

4.3. Surface-scanning

Two limbs of the mammoth (the left forelimb and the right shin and foot), both tusks, both nipples, the trunk, and the lower molars were scanned. The wool was not amenable to scanning because it lacked a discrete surface, so the part of the trunk that was covered by wool did not yield a usable model. We also encountered some difficulty in scanning the limbs and trunk due to the low reflectance of many surfaces. Nevertheless, our experiments with scanning parts of the mammoth were broadly successful. Scanning worked best on solid surfaces such as were presented by the tusks (Fig. 4A,C), for which our polygon-based models document the form and color of the originals and facilitate some measurements (light yellow annotations in Fig. 4C). Scanning parts of the body, including soft tissues, before defrosting and degradation provided baseline models for further work.

4.4. Computed tomography

The trunk and the distal part of the right hind leg of the mammoth were analyzed by computed tomography (Fig. 7). Using computed tomography, we were able to assess the condition of parts of the skeleton covered by soft tissues and even make measurements of bones surrounded by tissue (e.g., turquoise measurement of fibula length in Fig. 7D–467.3 mm). Using the CT scans, we also observed a small, fracture that partly detaches a flake of cortical bone from the surface of the tibia (marked by a yellow arrow in Fig. S7). This fracture is located on the posterior aspect of the tibia, and the retracted flake of cortical bone displaces associated soft tissues outward. Such a fracture would not have formed due to localized impact or compressive stresses on the hind limb as a whole. Rather, we recognize this as an avulsion fracture, a fracture that forms under extreme tensile loading produced by contraction

Table 2
Results of age, isotope, and elemental analyses of hair and bone (rib) of the Malolyakhovsky mammoth.

Laboratory nr.	Sample	age BP±1s	$\delta^{13}C$ (‰)	C%	$\delta^{15}N$ (‰)	N%	C/N
GrA-60021	hair	28,570 ± 150	−23.52	48.4	–	–	–
GrA-60044	bone	28,660 ± 160	−22.02	47.4	10.22	17.3	3.2

of muscles attempting to extend (ventroflex) the foot at the ankle. Given the nature of this fracture, it must have occurred before the animal's death.

Our CT scans of the tusks of the Malolyakhovsky mammoth revealed subtle but clear traces of annual increments of dentin apposition as shown in Fig. 8. This image summarizes information from the middle scan of the left tusk, with the tusk surface modeled in green. The box bounded by orange lines represents the stack of CT slices, of which one representative slice is indicated by the black plane in the middle of which, in grayscale, is a transverse section of the tusk with a clear concentric pattern of bright zones separated by darker zones. Each dark-light couplet represents one year of dentin apposition, where more nearly white zones (high X-ray attenuation) represent more highly mineralized dentin that tends to form in late winter, and darker zones (lower X-ray attenuation) form in spring-autumn (El Adli et al., 2016). The relatively abrupt transition from high to low attenuation thus marks the winter-spring boundary – our marker for the beginning and end of each year (Fisher, 1987, 1996; Fisher et al., 2014b; El Adli et al., 2015). The first year in any given transverse section is near the outer surface of the tusk, and subsequent years are located progressively nearer the central axis (Fisher, 1987, 1996). Individual years vary in thickness but in this specimen, years in the middle and proximal portions of the tusk tend to be 6–7 mm thick (measuring normal to incremental features). A succession of four annual increments has been "segmented" (i.e., distinguished volumetrically in the digital model of the specimen) and labeled in color – purple, yellow, blue, and red (the latter two are truncated by the end of this stack of slices), moving toward the proximal end of the tusk.

As noted in Methods, we sampled annual increments in terms of the average area they occupy in two representative longitudinal cross sections, rather than measuring their volume in the tusk as a whole. Fig. 9A shows one of two curved surfaces on which the area of annual dentin increments was measured. Both curved surfaces followed the structural axis of the tusk, and the second surface was locally perpendicular to the first. Fig. 9B shows a flattened representation of the curved, black surface in Fig. 9A, with conical, annual dentin increments (i.e., excluding cementum) traced out over most of the area illustrated. Fig. 9C shows the same area, without all of the increment boundaries traced, to make it easier to see the underlying pattern that must be followed. Once all

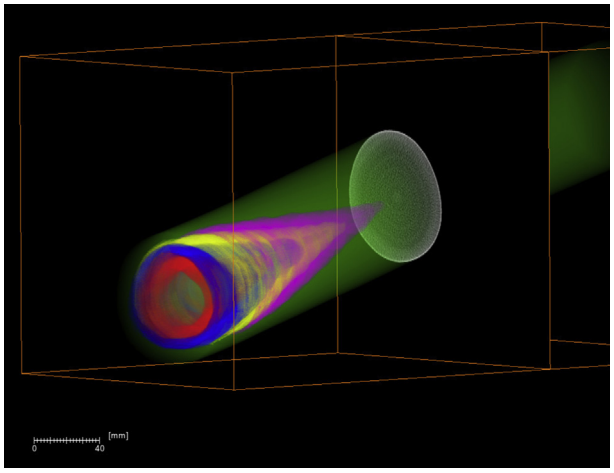

Fig. 8. Middle scan of left tusk of the Malolyakhovsky mammoth; orange box edges (print version shows grayscale only) indicate entire volume sampled by slice-data produced by CT scanning; near center of rectangular prism, one black slice from the series of scan slices shows a grayscale image of a transverse cross section with the concentric pattern of varying X-ray attenuation that distinguishes annual increments in tusk dentin; proximal to this slice, portions of four annual increments are segmented and color-coded as purple, yellow, blue, and red cones (in order of formation). (For interpretation of the references to colour in this figure legend, the reader is referred to the web version of this article.)

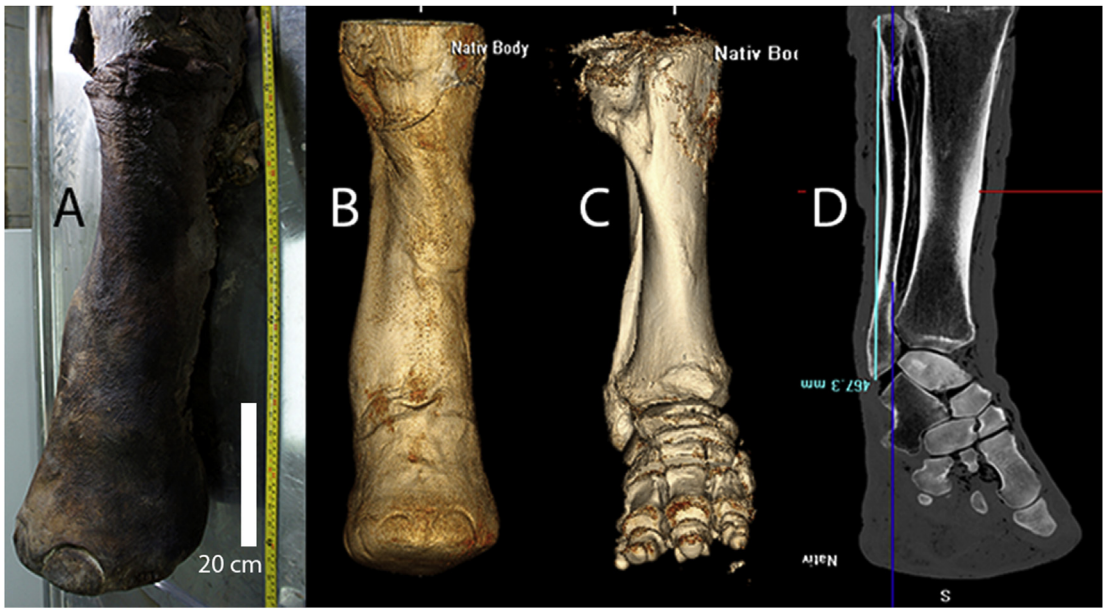

Fig. 7. Images of the right shin and hind foot of the Malolyakhovsky mammoth. A. Photograph of carcass surface, with 20-cm scale bar constructed based on tape measure in image. B. CT soft-tissue surface model of distal limb. C. Skeletal surface model of distal limb. D. Longitudinal section through tibia, fibula (length measured by turquoise line, 467.3 mm; light gray in print version), and foot. The avulsion fracture observed in tibia is not visible in this slice; see Supplemental material, Fig. S7.

boundaries on this surface were traced, the areas of successive annual increments were calculated and graphed as shown in Fig. 10, which then displays how annual increment area varies from one tusk-year to the next, over much of this female's lifetime. Our interpretation of this graph is explained in the Discussion section. Preliminary analysis of the right tusk showed a broadly similar pattern, but our CT data for this tusk were of lower resolution.

4.5. Hematology

The goal of this section was to characterize the dark brown liquid collected during the excavation of the Malolyakhovsky mammoth (2013) and determine whether it had any relation to the blood of the mammoth. For comparison, during dissection of the carcass in March 2014, we collected a swab from a blood vessel containing hemolyzed blood, removed from one of the forelimbs. Additional samples were collected for compositional analysis. This latter suite was numbered according to the time at which each thawed:

Sample 1: interstitial fluid (dark brown) from the anterior surface of the lower part of the left forelimb, taken on the first day of thawing (19 h, 03/11/14);
Sample 2: icy inter-fascial liquid from the anterior surface of the right upper forelimb (20 h, 03/11/14);
Sample 3: dark brown liquid substance, flowing out during thawing, (21 h, 03/11/14);
Sample 4: dark brown interstitial fluid from the anterior surface of the lower part of the right forelimb, taken on the second day of thawing (43 h, 03/12/14);
Sample 5: wrist bursa liquid from the left forelimb, taken on the third day of thawing (67 h, 3/13/14).

Our examination of fluid swabs sampling the dark brown liquid recovered during the excavation showed that the main background was gray-pink in color. This background was a homogeneous mass of destroyed, nucleus-free cellular elements that were morphologically similar to what is found in hemolyzed blood. Against this background we found individual cellular elements with the morphological configuration of blood cells of large mammals.

One common type of cellular element was intensely stained, with clear contours and diameters ranging from 5 to 7 μm. The cell plasmolemma was distinctly stained and thick. Basophilic cytoplasm was filled with dust-like grains and a preserved nucleus. Nuclear inclusions were deep purple in color and consisted of 4–6 segments. Some parts of the nucleus were connected by thin constrictions, and the nuclear chromatin had inhomogeneous, "lumpy" structure. We consider these polymorphonuclear leukocytes, or neutrophils.

Other cells were similar to lymphocytes, with a diameter of 3–4 μm, clear contours, basophilic cytoplasm, and a non-segmented nucleus. The structure of this was again inhomogeneous and "lumpy", and the nucleus had a rounded shape.

We also found concentrations of larger cells with diameters of 13–14 μm, precise contours, and irregular shapes. We identified these as monocytes. Their plasmalemma was thin, and their cytoplasm was basophilic (smoky-blue), with numerous dust-like granules. Their nuclei were large, polymorphic in form, and non-segmented. Chromatin was loose and irregular.

Our comparison swab, which sampled hemolyzed blood within a vessel from a forelimb had a background that stained smoky-blue. There were numerous clusters of destroyed cellular elements, but preserved cells were rare. Nevertheless, the cells we observed in these cases were identical to those of the dark brown liquid recovered during excavation. The similarity of these materials strongly suggests that the liquid recovered during excavation includes constituents of mammoth blood. Hematological analysis of material from the blood vessel yielded the characterization summarized in Table 3.

Many of the "destroyed cellular elements" noted above appeared to be remnants of red blood cells. During hemolysis, destruction of the erythrocyte membrane is accompanied by release of hemoglobin into the blood plasma. This suggested that hemoglobin was probably present in these samples, and this was confirmed by further hematological analysis (Table 4), although some values reported here for red blood cells are affected by the fact that we are dealing with blood that is massively hemolyzed. For example, the amount of hemoglobin may be informative, but mean corpuscular hemoglobin concentration is much higher than expected for a live animal.

Additional characterization of the samples taken during the thawing of the mammoth carcass required chemical analysis (Table S6), which showed that most of these samples had concentrations of iron ranging from 535.5 mmol/L to 2510.8 mmol/L. Iron content was not measured in the inter-fascial fluid, but it was notably low (2.7 mmol/L) in the synovial fluid. Neither of these samples were colored brown, nor would they be expected to have a close association with blood. The high concentration of iron in interstitial fluids is a plausible explanation for their dark brown color.

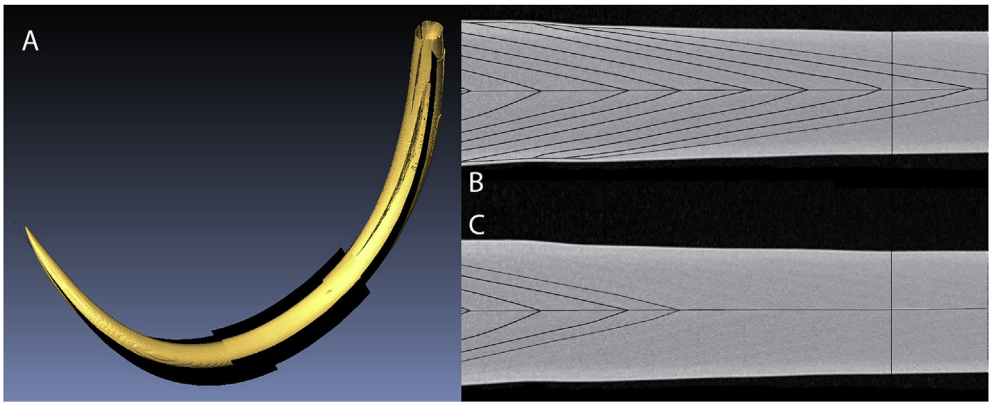

Fig. 9. Measuring annual increment area within tusks. A. Left tusk of the Malolyakhovsky mammoth with one curved surface (black) following the structural axis of the tusk. B. Flattened representation of curved surface in A, with winter-spring boundaries traced in black. C. Same as B, but with fewer winter-spring boundaries traced, revealing variation in attenuation that marks winter-spring boundaries.

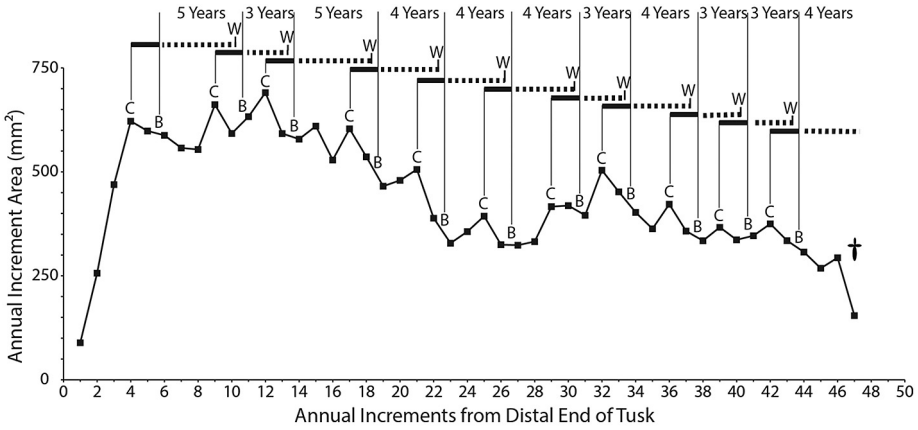

Fig. 10. Graph of annual increment areas (measured in longitudinal section, following the structural axis of the tusk) in the left tusk of the Malolyakhovsky mammoth vs. year in tusk; years numbered in order of formation, from distal end; plotted value is the average area for a given year, measured in two orthogonal planes, one of which (plane X) is the curved black surface in Fig. 9A and the other of which (plane Y) is another surface orthogonal to the first, also following the tusk axis. For the first three tusk years, increment area is severely reduced by abrasion, and only the larger increment area (measured on plane X or Y) is plotted, rather than the average. Years indicated by *C* (over the data point) are interpreted as years in which a calf was conceived (probably in late spring); years preceded by a *B* (offset above and just to the left of corresponding data point) are interpreted as the first year of a calf (i.e., immediately following this calf's birth, just before the vegetational winter-spring boundary; Rountrey et al., 2012). Inferred calving history for this individual is indicated schematically above the area vs. year graph, with solid horizontal lines marking a succession of 20- to 22-month gestation periods (Fisher et al., 2014a) and the dashed, horizontal continuation of each pregnancy indicating the likely nursing interval for this calf (Cherney, 2015). This tusk growth record suggests a lifetime reproductive output of at least eleven calves, with an inter-birth interval averaging about 4 years. Dagger symbol at right marks year of death.

Investigation of urea and creatinine showed high concentrations in all samples (38.44–116.35 mmol/L and 76.0–274.4 mmol/L, respectively), except for the synovial fluid from the forelimb (wrist) bursa. These characteristics are probably indicative of the process of decomposition, accompanied by production of nitrogen-containing substances. Biochemical studies also confirmed the presence of enzymes (Table S6). We interpret their origin as related to the activity of microbes involved in the initiation of carcass decomposition.

4.6. Histology

In serial histological sections of collagen and muscle fiber, we observed well preserved arterial and venous blood vessels of all sizes. These were easily recognized from the hemolyzed blood clot within each vessel. At high magnification within these blood clots, we observed erythrocyte "ghosts" (i.e., faint outlines that we interpret as remains of erythrocytes; Fig. S8A in Supplemental material), confirming the original presence of blood.

In some sections, we observed muscle fiber bundles in longitudinal, transverse, and oblique orientations, indicating a multidirectional arrangement of these bundles. Chains of elongate dark spots located along the muscle fibers are clearly visible on longitudinal and transverse sections of muscle bundles. We suspect these are deformed myosymplast nuclei located under the sarcolemma (Fig. S8B).

In subcutaneous tissue samples from the proboscis we observed well-preserved concentrations of adipose tissue in the form of clusters of adipocytes with no cytoplasm inside the preserved cell membrane. These were also observed with the inverted microscope we used at the beginning of our study (Garmaeva et al., 2014). Stratified squamous epithelium with deep non-keratinous epithelial crests is well preserved along the dorsal ridge of the mammoth trunk where thin basement membrane and epithelial cells of the basal and spinous layers are differentiated.

Comparing structures seen across all samples of trunk tissue, we observe the best preservation in the distal trunk. For a broader comparison, we have begun to study samples identified (on gross morphological and anatomical grounds; see above) as coming from liver, stomach, intestines, diaphragm, and pericardium, but results of these studies are not yet available.

4.7. Microbiology

In all, 34 bacterial isolates were cultivated from intestinal contents, bone marrow, and contents of a gingival pocket of a lower molar. Four taxa were identified by biochemical characteristics and 16S rDNA sequencing (Table 5).

The genomes of two strains of isolated enterococci (*Enterococcus faecium* and *Enterococcus hirae*) were sequenced, and draft genomes were deposited in Genbank under accession numbers

Table 3
Hematological indices for material from a blood vessel recovered during thawing of the Malolyakhovsky mammoth.

Defined parameters	Indices
WBC: White blood cell count (x10^3 cells/micro-L)	1.6 x 10^9/L
WBCP: White blood cell count from peroxidase method (x10^3 cells/micro-L)	1.4 x 10^9/L
NEUT: Absolute count of neutrophils (x10^3/micro-L)	0.2 x 10^9/L
LYMPH: Absolute count of lymphocytes (x10^3/micro-L)	0.8 x 10^9/L
MONO: Absolute count of monocytes (x10^3/micro-L)	0.2 x 10^9/L
NEUT %: Percent of neutrophils	11.9%
LYMPH %: Percent of lymphocytes	54.6%
MONO %: Percent of monocytes	15.5%

Table 4
Hemoglobin indices for material from a blood vessel recovered during thawing of the Malolyahovsky mammoth.

Defined parameters	Indices
HGB: Hemoglobin (g/dL)	22
RBC: Red blood cell count (x10^6 cells/micro-L)	0.03 x 10^9/L
HCT: Hematocrit (%)	0.2
MCV: Mean corpuscular volume (fL)	67.3
MCH: Mean corpuscular hemoglobin (pg)	862.9
CH: Cellular hemoglobin concentration (pg)	15.8
MCHC: Mean corpuscular hemoglobin concentration (g/dL)	12831
CHCM: Corpuscular hemoglobin concentration mean (g/dL)	243 g/L

LGAN00000000 and LGAO00000000. The characteristics of the genome of *Enterococcus faecium 58m*, including the presence of genes associated with pathogenic potential, were discussed by Goncharov et al. (2016). Also *Carnobacterium maltaromaticum* was isolated from the mammoth's bowel.

Results of the intestinal microbiome taxonomic analysis are shown in Fig. S9 (Supplemental material). The vast majority (58.48%) of species in the intestinal microbiome were Gammaproteobacteria. The percentage of *Bacilli, Flavobacteria, Clostridia, Actinobacteria, Betaproteobacteria, Bacteroidia* was 15.02%, 8.35%, 8.07%, 3.19%, 2.29% and 1.84%, respectively. The majority of microorganisms represented the family *Pseudomonadaceae*. We obtained 15,038 sequences over 280 bp long.

5. Discussion

One of the main issues that interested us in this specimen from the beginning was the likelihood that it was a female. The circumference of each tusk, especially as it varied with distance from the tip (Supplemental material, Table S1) was the first cue supporting this interpretation. The tusks of an adult male would have had greater maximum girth and would have increased girth more rapidly with distance from the tip (Fisher, 2007, 2008; Smith and Fisher, 2011), instead of stabilizing girth only a little beyond the first meter from the tip. The left and right tusk of this specimen have slightly different girth profiles, but this is mostly due to the difference of about 20 cm in their lengths, reflecting greater loss of tusk material from the right tusk by tip fracture and abrasion. This in turn was why the left tusk was a better candidate for life history reconstruction; it contained at least some record of years near its tip that were not preserved in the right tusk. The early years in each tusk could only be directly observed in the CT record, but the length difference was enough to expect a difference in the number of tusk-years preserved.

In addition to the girth profile, another trait consistently associated with adult females, especially in their later stages of life, is possession of pulp cavities shorter than those of similar-age males and much shorter than the depth of the alveolus (Smith and Fisher, 2011). For comparison with the Malolyakhovsky mammoth, the Yukagir mammoth, an adult male of about the same age, has a right tusk 316.4 cm long on its outside curve, a maximum girth of 45.6 cm, near the alveolar margin, and a pulp cavity depth of 26 cm (Mol et al., 2007), all values greater than what we report in Results. Finally, the annual dentin increment thicknesses observed for Malolyakhovsky contrast with thicknesses up to 8.7 mm observed on the Yukagir mammoth, which was actually living at a time (near the Last Glacial Maximum) with a more severe climate (Fisher et al., 2010).

The discovery of well-developed mammae with nipples on the anteroventral aspect of the thorax also confirmed that this mammoth was female. Patent milk ducts on the left nipple suggest that this individual was still nursing, or had just recently weaned a calf at the time of her death. In addition, her relatively small body size (which of course has to be considered in terms of age, discussed below) is also consistent with identification as female. Both the Malolyakhovsky mammoth and the Yukagir mammoth (Mol et al., 2007) had well-preserved front feet on which a complete circumference could be measured, and from which an estimate of shoulder height could be calculated. Moreover, the Yukagir mammoth preserved elements of an entire forelimb, facilitating a direct measurement that confirmed use of the ratio originally observed for *Elephas maximus* (Sukumar et al., 1988). The Yukagir mammoth, with a shoulder height of about 290 cm, was about 21% larger in this lineal dimension than the Malolyakhovsky mammoth, with a shoulder height of 240 cm. This difference is normal for the degree of sexual dimorphism in proboscideans (Smith and Fisher, 2013).

As for age, the fact that all epiphyses in the limbs and axial skeleton are fused is a direct indication that this animal had achieved its determinate stature. For females, this suggests a minimum age of 30 (or even a few years younger; Lister, 1999), but a better approximation comes in this case from dental evidence. As reported above, the lower molars are apparently m3s in only a moderate state of wear. The Laws (1966) age determination of ca. 47 years is based on the timing of eruption and wear in African elephants, which could differ from mammoths. Asian elephants might represent a more appropriate model, and available information (Roth and Shoshani, 1988) is compatible with ages in the range of 50–60, but the resolution is low.

As reported in Results, identification of the upper molars is less clear. These teeth are smaller than expected, given the lowers, and much more heavily worn. We considered a hypothesis that these might be malformed M2s that did not advance through the maxillae normally because of their contorted form and were not followed by normal M3s (leaving questions of cause and effect aside). This would at least explain the advanced stage of wear on the uppers (which Laws, 1966, describes as usually less heavily worn than associated lowers) as a result of successive interaction with both m2s and m3s. Although we cannot rule this hypothesis out, it seems less parsimonious than the alternative hypothesis that the upper molars are simply malformed M3s that suffered excessive attrition because of their abnormal morphology, losing much of the anterior part of each before lowers were comparably advanced in wear. Additional asymmetries in the mandible and lower dentition may also be involved, but none of these issues impact our age assessment.

A more direct approach to determining age is to count the number of years identified in the CT data. In the left tusk we observed parts of 47 years (with several fewer in the right tusk) so the animal was at least this old. As is widely recognized (Fisher, 1996; Haynes, 2016), tusks are subject to breakage and abrasion at their tips, so in an animal this old, the record of tusk-years is doubtless incomplete. The first three years in the left tusk are already severely reduced in cross sectional representation, and earlier years are lost altogether. Fortunately, concurrent studies of juvenile woolly mammoths have allowed us provisionally to distinguish tusks of males and females and characterize patterns of tusk growth from before birth, up to an age of about 13 (Rountrey et al., 2007; Rountrey, 2009; Cherney, 2015). Comparing tusk girth profiles in these animals with the tip of the left tusk of the

Table 5
16S rDNA analysis of bacterial isolates.

Isolate	Origin	Closest relative (16S rRNA)	% 16S rRNA similarity
1	intestinal contents	*Carnobacterium maltaromaticum*	99
2	intestinal contents	*Enterococcus faecium*	98
3	intestinal contents	*Enterococcus hirae*	98
4	gingival pocket	*Enterococcus faecium*	99
5	bone marrow	*Arthrobacter* sp.	97

Malolyakhovsky mammoth allows us to estimate that about 8–10 years are missing from the tip of this specimen. We therefore propose that this individual was about 55 years old at death.

In terms of condition at the time of death, we suspect this animal was at least reasonably healthy. The $\delta^{13}C$ value of −23.52‰ (VPDB) reported in Table 2 in conjunction with our AMS age estimate is a "bulk" value from bone (undergoing remodeling) that might characterize the last decade or more of life, but it is close to what we expect for a high-latitude browser/grazer (without access to C_4 vegetation) dependent on fat reserves for at least part of the year (e.g., Bocherens, 2003; Gohman et al., 2010). Likewise, the $\delta^{15}N$ value of 10.22‰ (AIR) is normal for Siberian mammoths (Bocherens et al., 1996; Szpak et al., 2010). The amount of fat preserved on parts of the body is also suggestive of generally good condition. The intestinal contents that we retrieved from this animal, and that were partly analyzed in our microbiological studies, also represent an opportunity for new information on mammoth diets, but unfortunately, we have not yet undertaken this work.

Another issue we attempted to resolve is the cause and timing of this individual's death. The presence of clean ice around most of the carcass implies that the body ended up surrounded by water, whether before or after death. This suggests that the body was in a highly localized depression of some sort on the tundra surface. It seems more likely that the animal fell into this depression and became trapped than that its body was somehow introduced into such a depression after death. If only because depressions of moderate depth are more likely to be encountered on the tundra surface than much deeper ones, we suspect that the depression may never have been large enough to cover the entire body, but it must have been something from which the animal could not extricate itself. The hematoma on the right flank is a clear sign of perimortem trauma, but it could have been sustained during the fall into the depression, or in an encounter with predators that immediately preceded entrapment. In this sense, an encounter with predators could have been responsible for the lack of caution that resulted in entrapment. The avulsion fracture on the posterior aspect of the tibia could reflect a frantic attempt by the mammoth to lurch upward, out of the depression into which it had fallen, with extensor muscles of the hind foot contracting vigorously in "full panic" mode. Capping this grim scene off, blood in the hair and surrounding ice and chunks of tissue in the ice around the body suggest that the upper part of the mammoth was eaten by predators, probably starting when it was still alive. Many bones from the upper part of the body are missing, and many of those recovered showed signs of gnawing. At this time, we cannot distinguish damage and removal due to ancient predation from effects of Recent scavenging, but both likely occurred.

We suspect that the season of death was late summer-early autumn, because the preserved short hair had not yet been replaced by what could be recognized as winter fur, and because of the remains of green plants in surrounding ice. This hypothesis could be tested by microscopic tusk analysis. With the arrival of autumn, the carcass and its surroundings would have frozen solid. Subsequent aggradation of the tundra surface during the Last Glacial Maximum may have also played a role in protecting this carcass, In addition, the ice immediately around the body would have deformed readily under the usual pressures generated within permafrost, protecting the body from extrinsic forces and leaving it with a normal shape, compared to the flattened carcasses of most other permafrost finds. Despite a history that favored preservation in so many ways, Recent melting of the permafrost subjected the carcass once again to exposure, decomposition, and scavenging.

Earlier work on patterns of tusk growth and their relation to life history showed evidence that tusk growth in adult female proboscideans might be "pulsed" in a manner that could reflect the history of calving cycles (Fisher, 1996, 2009; Fisher et al., 2008). During a year when an adult female was pregnant or nursing a calf, she would have less calcium or phosphate to commit to tusk growth, and thus annual increment volume, and area, would be expected to be smaller. Dentin apposition, dentin extension, and the process of tusk eruption (which requires remodeling of the periodontal ligament and thus access to protein; Fisher, 2008; El Adli et al., 2015) all represent processes that in some sense compete with the needs of a fetus or newborn calf. Fig. 10 shows such a cyclical pattern of variation in increment area in the left tusk of the Malolyakhovsky mammoth, and we suspect this represents calving cycles. In the last decade of life, this pattern is somewhat subdued, and year area is reduced, possibly reflecting the decline in occlusal surface area of the upper molars, which would have reduced their ability to process food effectively.

The labels on Fig. 10 indicate a provisional interpretation of how portions of calving cycles correspond to the cycle of variation in tusk growth. Each data point on this curve expresses the cumulative tusk growth of a complete year. As such, time along the curve is essentially focused at data points, even though tusk growth is continuous, notwithstanding variation in rate. We interpret conception as occurring during most years showing a peak value in area, marking the beginning of a cycle. Only three local maxima exist on this curve that are not interpreted as conceptions (at years 15, 30, and 46), and we return to these below. As explained above, our annual increments run from one winter-spring boundary to the next. Based on evidence of musth (periods of male mating activity), and thus conception, in early summer (Fisher et al., 2010), calf birth occurring before the onset of vegetation growth in spring (Rountrey et al., 2012), and a gestation period that might be slightly shorter than that of extant elephants (Maschenko, 2002; Fisher et al., 2014a), which is usually 22 months (Moss, 1988), we mark conception (*C*, in Fig. 10) just above a local maximum in area (i.e., in the early portion of that year). For two years following peaks in area, tusk growth generally declines because of the demand for fetal calcium, phosphate, and protein (only two exceptions, in years 11 and 41), and to reflect a gestation period just under two years, we place the *B* for birth just above and to the left of the second year following conception. From both *C* and *B* markers in Fig. 10, fine lines lead up to points along a continuous time-line where the phases of successive calving cycles (stepping downward toward the right) are marked as solid horizontal lines (gestation of each calf) and dashed horizontal lines (nursing of each calf). The normal pattern in extant elephants (Moss, 1988), and we suspect in woolly mammoths as well (Rountrey et al., 2007; Cherney, 2015), is for calves to be nursed until just before the birth of the next calf. Weaning is therefore marked by *W* on the time-line of calving cycles, shortly before the next *B* (Fig. 10). Following birth, the continuing demand of lactation also suppresses tusk growth, but this diminishes with time, as the calf's milk intake decreases, leading up to the next opportunity for conception.

Two cycles that we regard as almost archetypical are the ones from tusk-year 17 to tusk-year 21 and from tusk-year 21 to 25. Both the direction and the approximate magnitude of change during these cycles are similar. The next cycle (25–29) is again similar, though it does not lead to as great an overall decline in area. These in turn are relatively closely matched by other cycles in this record of tusk growth. Of the three local maxima in annual increment area that are not recognized as years of conception, the first, tusk-year 15, is followed in tusk-year 17 by another local maximum with a more recognizable pattern following it. Conceptions in both tusk-years 15 and 17 are incompatible with a healthy calf from the first, so we have provisionally added the two years between 15 and 17 to the previous cycle. The second local maximum not counted as a conception is for tusk-year 30, where area is in fact barely larger

than in the previous year, so this seems more likely to reflect a pregnancy with lower than usual calcium and phosphate demand, a pattern to which we return below. Finally, the last local maximum not interpreted as a year of conception is tusk-year 46, where death intervenes and precludes recognition of a full cycle. Alternatively, the drop in annual increment area from tusk year 46–47 is so precipitous that this could reflect a decline in condition related to loss of occlusal surface area due to attrition of the upper molars, following which, this female might not have been able to carry a pregnancy to term even if she had been able to conceive.

The only other anomalies on this graph are two cases in which the normal decline in annual increment area is not sustained throughout pregnancy, in tusk-years 11 and 41. Each of these cases could be interpreted as instances in which low birth weight of a calf resulted in less demand for calcium and phosphate than in other cycles. Alternatively, perhaps these pregnancies were not carried to term. These cases correspond to two of only four instances of calving cycles as short as three years, and the other two instances of three-year cycles involve intervals without a marked overall decline. These cases contrast with the two instances in this life history where calving cycles are as long as five years, from tusk-year 4 to 9 and from tusk-year 14 to 19. Over both of these five-year calving cycles and the pregnancies preceding them, there is a marked decline in increment area, reflecting a large demand for calcium and phosphate.

Lee and Moss (1986) have shown that African elephant mothers provision their male calves more generously than their female calves, a strategy that would be selected for under circumstances where the variance in male reproductive success (often dependent on body size) is greater than the variance in female reproductive success. This difference is expected under the social structure and mating behaviors documented in elephants and suspected in mammoths (Fisher, 1996, 2009). As a result, it would be plausible to propose that the two five-year calving cycles involved male calves, and at least two (or as many as all four) of the three-year calving cycles involved female calves. This leaves at least four four-year cycles (not counting the one terminated by death) for which the sex of the calf cannot be determined in this way. All told, the tusk growth record for this individual shows patterns that tend to repeat relatively consistently, and that appear to correspond to documented features of elephant life history.

The average calving cycle for this individual seems to be about four years long. With forty-seven years in the tusk record and 8–10 years missing from the tip, this tusk record probably extends from when the animal was just reaching maturity to its death in its mid- to late fifties. This record suggests a lifetime output of at least eleven calves, with most possibly surviving until weaning (unless we interpret some of the short cycles as calf losses; Fisher, 1996). This level of fecundity, and calving intervals of this relative brevity (compared to African elephants experiencing drought stress; Moss, 1988) suggests that on the scale of a lifetime, environmental stress was not severe.

The dark brown liquid encountered during excavation of the Malolyakhovsky mammoth is not “blood” in the same sense as the solid hematoma on the mammoth's right flank, or the hemolyzed contents of blood vessels distributed over many parts of the carcass. At the same time, our analyses showed that this liquid contains abundant cellular debris, including neutrophils, lymphocytes, and monocytes containing nuclear inclusions, that were all derived from blood. In addition, the dark brown color of this liquid is associated with a high iron content, and that in turn is probably derived from hemoglobin released by breakdown of erythrocyte membranes. We do not yet know how the composition of this liquid affected its freezing point, but this liquid was at least derived in part from degraded mammoth blood. The concentration of hemoglobin found in this specimen seems high (22 g/dL) compared to reference values for extant African elephants (10–16 g/dL; Zoo Information Management System, http://www2.isis.org/), but before attributing great significance to this, we should seek additional comparative data and carefully assess the consequences of massive hemolysis on our specimen.

One hallmark of the excellent preservation noted on this specimen was that remains of nuclei of white blood cells were common in our hematological investigations, in contrast to the rarity of preserved nuclei in studies of other specimens (e.g., Papageorgopoulou et al., 2015). Likewise, many tissue samples on this specimen showed excellent preservation. On the trunk, the distal extremity showed better histological conditions than more proximal regions, probably because this part of the trunk was not subject to as many cycles of freezing and thawing. Good preservation of organics is also implied by the C/N ratio reported in Table 2(3.2), which is well within the bounds determined for modern bone (2.9–3.6; DeNiro, 1985).

We suspect that the microbial community documented by our research is typical for the gut microbiota of herbivores, but more comparative analysis is needed. The predominance of Pseudomonadaceae is of interest, due to the ice nucleation capability of some pseudomonads (Bisht et al., 2013) and their ability to produce cryoprotectant agents (Carrión et al., 2015). We suspect that such properties, conferred by pseudomonads in the intestinal tract of the mammoth, promoted the good preservation of her tissue.

Although relatives of *Pseudomonas* are not the dominant group in the intestinal microbiome of most animals, *Pseudomonas* was dominant in the microbiome of the young mammoth named Lyuba (Mardanov et al., 2012). Mardanov et al. hypothesized that this was due to Lyuba's diet being dominated by milk (some species of Pseudomonadaceae cause souring of dairy products). However, we observed Pseudomonadaceae to be dominant in an adult animal, suggesting a more general association of this group of microorganisms with the mammoth's digestive tract. Unlike Lyuba's microbiome, there was also a significant percentage of Firmicutes.

Some of the isolated *Carnobacterium* strains could also be linked to conservation of the Malolyakhovsky mammoth's carcass. It is known that these bacteria can produce preservative substances. It has been shown that carnobacteriocins and their producer, *Carnobacterium maltaromaticum*, are candidate food biopreservative agents for exploration of preservation strategies that suppress or reduce the growth of bacterial pathogens and bacteria with high spoilage potential (O'Sullivan et al., 2002). Likewise, the ability of *Carnobacterium* spp. to survive in extreme environments, including frozen soils, has been discussed previously (Nicholson et al., 2013).

6. Conclusion

This carcass of a mammoth from Maly Lyakhovsky Island presents a remarkable opportunity to compare numerous sources of data on the life of this animal. Even though its body has been almost half destroyed, the quality of what remains, at the level of cells and tissues, makes it the best-preserved specimen of an adult female woolly mammoth ever discovered. The animal appears to have been trapped in a depression that accommodated about half the body volume. Water was probably already present in this depression and froze, preserving part of the carcass. The carcass remained in excellent condition for thousands of years because the severe climatic conditions of the Arctic islands kept it locked inside almost pure ice that never melted.

Association of soft and hard tissues has given us an opportunity to conduct a detailed CT analysis of the tusks of a confirmed adult female mammoth. Within tusk dentin we find regular cycles of variation in X-ray attenuation that we interpret as reflecting the

history of tusk growth. Some variation in rates of growth would be expected in any such system, but measurements of the longitudinal cross sectional area of annual increments suggest a pulsed pattern of growth with a period of about four years. We interpret this as a calving history for this female, implying a normal birth interval of about four years, comparable to calving intervals of extant elephants living under reasonably favorable conditions. We look forward to new opportunities to test these methods on other specimens. If confirmed, data on calving intervals for woolly mammoths would contribute greatly toward understanding the levels and sources of stress on these animals during the millennia leading up to their ultimate extinction.

Acknowledgments

Aspects of the recovery and analysis of this specimen were supported by North-Eastern Federal University, Yakutsk. The microbiological research and 16S rRNA sequencing of the microbiome was supported by the research resource center “Molecular and cell technologies” of St. Petersburg State University and by grant 16-04-01737A to A.E. Goncharov, from the Russian Foundation for Basic Research. Funding sources had no role in study design or preparation of this publication. We are grateful to Igor Sleptsov, whose cooperation was fundamental to the initial discovery and subsequent recovery of this mammoth. S.G. Beld greatly improved most of our illustrations, and R. Berlinski (Toledo Zoo) provided ZIMS reference data for *Loxodonta africana*. We are especially thankful for the detailed and helpful suggestions we received from two anonymous reviewers. We are likewise pleased to acknowledge the editors for their helpful recommendations and assistance.

Appendix A. Supplementary data

Supplementary data related to this article can be found at http://dx.doi.org/10.1016/j.quaint.2017.01.007.

References

Bisht, S.C., Joshi, G.K., Haque, S., Mishra, P.K., 2013. Cryotolerance strategies of Pseudomonads isolated from the rhizosphere of Himalayan plants. Springerplus 2, 667. http://dx.doi.org/10.1186/2193-1801-2-667.

Bocherens, H., 2003. Isotopic biogeochemistry and the paleoecology of the mammoth steppe fauna. In: Reumer, W.F., de Vos, J., Mol, D. (Eds.), Advances in Mammoth Research, Proceedings of the 2nd International Mammoth Conference, Deinsea, vol. 9, pp. 57–76.

Bocherens, H., Pacaud, G., Lazarev, P.A., Mariotti, A., 1996. Stable isotope abundances (^{13}C, ^{15}N) in collagen and soft tissues from Pleistocene mammals from Yakutia: implications for the palaeobiology of the Mammoth Steppe. Palaeogeography, Palaeoclimatology, Palaeoecology 126, 31–44.

Boeskorov, G.G., Tikhonov, A.N., Lazarev, P.A., 2007a. A new find of a mammoth calf. Dokl. Biol. Sci. 417, 480–483.

Boeskorov, G.G., Tikhonov, A.N., Suzuki, N. (Eds.), 2007b. The Yukagir Mammoth. Institute of Applied Ecology of the North [Yakutsk], St. Petersburg.

Boeskorov, G.G., Potapova, O.R., Maschenko, E.N., Protopopov, A.V., Kuznetsova, T.V., Agenbroad, L., Tikhonov, A.N., 2014. Preliminary analyses of the frozen mummies of mammoth (*Mammuthus primigenius*), bison (*Bison priscus*) and horse (*Equus* sp.) from the Yana-Indigirka lowland, Yakutia, Russia. Integr. Zool. 9, 471–480.

Carrión, O., Delgado, L., Mercade, E., 2015. New emulsifying and cryoprotective exopolysaccharide from Antarctic *Pseudomonas* sp. ID1. Carbohydr. Polym. 117, 1028–1034. http://dx.doi.org/10.1016/j.carbpol.2014.08.060.

Cherney, M.D., 2015. Records of Growth and Weaning in Fossil Proboscidean Tusks as Tests of Pleistocene Extinction Mechanisms. University of Michigan, USA. PhD dissertation.

DeNiro, M.J., 1985. Postmortem preservation and alteration of in vivo bone collagen isotope ratios in relation to palaeodietary reconstruction. Nature 317, 806–809.

El Adli, J.J., Cherney, M.D., Fisher, D.C., Harris, J.M., Farrell, A.B., Cox, S.M., 2015. Last years of life and season of death of a Columbian mammoth from Rancho La Brea. In: Harris, J.M. (Ed.), La Brea and beyond: the Paleontology of Asphalt-preserved Biotas. Natural History Museum of Los Angeles County, Science Series, vol. 42, pp. 65–80.

El Adli, J.J., Fisher, D.C., Vartanyan, S.L., Tikhonov, A.N., 2016. Final years of life and seasons of death of woolly mammoths from Wrangel Island and mainland Chukotka, Russian Federation. Quat. Int. 445, 135–145. http://dx.doi.org/10.1016/j.quaint.2016.07.017.

Fisher, D.C., 1987. Mastodont procurement by Paleoindians of the Great Lakes region: hunting or scavenging? In: Nitecki, M.H., Nitecki, D.V. (Eds.), The Evolution of Human Hunting. Plenum, New York, pp. 309–421.

Fisher, D.C., 1996. Extinction of proboscideans in North America. In: Shoshani, J., Tassy, P. (Eds.), The Proboscidea: Evolution and Palaeoecology of Elephants and Their Relatives. Oxford University Press, Oxford, pp. 296–315.

Fisher, D.C., 2007. Life history analysis of the Yukagir mammoth. In: Boeskorov, G.G., Tikhonov, A.N., Suzuki, N. (Eds.), The Yukagir Mammoth. Institute of Applied Ecology of the North [Yakutsk], St. Petersburg, pp. 142–156.

Fisher, D.C., 2008. Taphonomy and paleobiology of the Hyde Park mastodon. In: Allmon, W.D., Nester, P.L. (Eds.), Mastodon Paleobiology, Taphonomy, and Paleoenvironment in the Late Pleistocene of New York State: Studies on the Hyde Park, Chemung, and North Java Sites. Palaeontographica Americana, vol. 61, pp. 197–289.

Fisher, D.C., 2009. Paleobiology and extinction of proboscideans in the Great Lakes region of North America. In: Haynes, G. (Ed.), American Megafaunal Extinctions at the End of the Pleistocene. Springer Science+Business Media, New York, pp. 55–75.

Fisher, D.C., Beld, S.G., Rountrey, A.N., 2008. Tusk record of the North Java mastodon. In: Allmon, W.D., Nester, P.L. (Eds.), Mastodon Paleobiology, Taphonomy, and Paleoenvironment in the Late Pleistocene of New York State: Studies on the Hyde Park, Chemung, and North Java Sites. Palaeontographica Americana, 61, pp. 417–463.

Fisher, D.C., Rountrey, A.N., Beld, S.G., Fox, D.L., Gohman, S.C.L., Tikhonov, A.N., Mol, D., Buigues, B., Boeskorov, G.G., Lazarev, P.A., 2010. Life history of the Yukagir mammoth. In: Lazarev, P.A., Boeskorov, G.G., Maschenko, E. (Eds.), Proceedings of the IVth International Mammoth Conference, Institute of Applied Ecology of the North, Yakutsk, pp. 54–63.

Fisher, D.C., Tikhonov, A.N., Kosintsev, P.A., Rountrey, A.N., Buigues, B., van der Plicht, J., 2012. Anatomy, death, and preservation of a woolly mammoth (*Mammuthus primigenius*) calf, Yamal Peninsula, northwest Siberia. Quat. Int. 255, 94–105.

Fisher, D.C., Shirley, E.A., Whalen, C.D., Calamari, Z.T., Rountrey, A.N., Buigues, B., Lacombat, F., Grigoriev, S.E., Lazarev, P.A., 2014a. X-ray computed tomography of two mammoth calf mummies. J. Paleontology 88 (4), 664–675.

Fisher, D.C., Cherney, M.D., Newton, C., Rountrey, A.N., Calamari, Z.T., Stucky, R.K., Lucking, C., Petrie, L., 2014b. Taxonomic overview and tusk growth analyses of Ziegler Reservoir proboscideans. Quat. Res. 82 (3), 518–532.

Garmaeva, D., Buzinaeva, M., Savvinov, G., Grigoriev, S., Fedorov, S., Tikhonov, A., Novgorodov, G., Cheprasov, M., 2014. Histological evaluation of tissue structure preservation in the Malolyakhovski mammoth. In: Abstract Book of the VIth International Conference on Mammoths and their Relatives S.A.S.G., vol. 102, p. 63.

Garutt, V.E., Foronova, I.V., 1976. A Study of Teeth of Ancient Elephants. Methodological Recommendations. Novosibirsk (in Russian).

Gohman, S.C.L., Fox, D.L., Fisher, D.C., Vartanyan, S.L., Tikhonov, A.N., Mol, D., Buigues, B., 2010. Paleodietary and paleoenvironmental implications of carbon and nitrogen isotopic variations in late Pleistocene and Holocene tusks of *Mammuthus primigenius* from Northern Eurasia. In: Lazarev, P.A., Boeskorov, G.G., Maschenko, E. (Eds.), Proceedings of the IVth International Mammoth Conference, Institute of Applied Ecology of the North, Yakutsk, pp. 177–187.

Goncharov, A., Grigorjev, S., Karaseva, A., Kolodzhieva, V., Azarov, D., Akhremenko, Y., Tarasova, L., Tikhonov, A., Marsharkiy, A., Zueva, L., Suvorov, A., 2016. Draft genome sequence of *Enterococcus faecium* strain 58m, isolated from intestinal tract content of a woolly mammoth, *Mammuthus primigenius*. Genome Announc. 4 (1) http://dx.doi.org/10.1128/genomeA.01706-15 e01706–e015.

Haynes, G., 2016. Finding meaning in mammoth age profiles. Quater. Inter. 443, (Part A), 65–78. http://dx.doi.org/10.1016/j.quaint.2016.04.012.

Kosintsev, P.A., Lapteva, E.G., Trofimova, S.S., Zanina, O.G., Tikhonov, A.N., Van der Plicht, J., 2012. Environmental reconstruction inferred from the intestinal contents of the Yamal baby mammoth Lyuba (*Mammuthus primigenius* Blumenbach, 1799). Quat. Int. 255, 231–238.

Laws, R.M., 1966. Age criteria for the African elephant, *Loxodonta a. africana*. East Afr. Wildl. J. 4, 1–37.

Lee, P.C., Moss, C.J., 1986. Early maternal investment in male and female African elephant calves. Behav. Ecol. Sociobiol. 18, 353–361.

Lister, A.M., 1999. Epiphyseal fusion and postcranial age determination in the woolly mammoth *Mammuthus primigenius*. In: Haynes, G., Klimowicz, J., Reumer, J.W.F. (Eds.), Mammoths and the Mammoth Fauna: Studies of an Extinct Ecosystem. Deinsea, vol. 6, pp. 79–88.

Lister, A.M., Sher, A.V., 2015. Evolution and dispersal of mammoths across the Northern Hemisphere. Science 350 (6262), 805–809.

Maglio, V.J., 1973. Origin and evolution of the Elephantidae. Trans. Am. Philosophical Soc. N. S. 63 (3), 149.

Mardanov, A.V., Bulygina, E.S., Nedoluzhko, A.V., Kadnikov, V.V., Beletskii, A.V., Tsygankova, S.V., Tikhonov, A.N., Ravin, N.V., Prokhorchuk, E.B., Skryabin, K.G., 2012. Molecular analysis of the intestinal microbiome composition of mammoth and woolly rhinoceros. Dokl. Biochem. Biophys. 445, 203–206. http://dx.doi.org/10.1134/S1607672912040060.

Maschenko, E.N., 2002. Individual development, biology and evolution of the woolly mammoth. Cranium 19, 1–120.

Maschenko, E.N., Protopopov, A.V., Plotnikov, V.V., Pavlov, I.S., 2013. Specific characters of the mammoth calf (*Mammuthus primigenius*) from the Khroma River (Yakutia). Biol. Bull. 40, 626–641.

Mol, D., Coppens, Y., Tikhonov, A.N., Agenbroad, L.D., MacPhee, R.D.E., Flemming, C., Greenwood, A., Buigues, B., de Marliave, C., van Geel, B., van Reenen, G.B.A., Pals, J.P., Fisher, D.C., Fox, D., 2001. The Jarkov mammoth: 20,000-year-old carcass of a Siberian woolly mammoth *Mammuthus primigenius* (Blumenbach, 1799). In: Cavarretta, G., Giola, P., Mussi, M., Palombo, M.R. (Eds.), Proceedings of the First International Congress, "The World of Elephants", Consiglio Nazionale Delle Ricerche, Roma, pp. 305–309.

Mol, D., Shoshani, J., Tikhonov, A.N., Boeskorov, G.G., Lazarev, P.A., Agenbroad, L., Suzuki, N., Buigues, B., 2007. Anatomic-morphological features and individual age of the Yukagir mammoth. In: Boeskorov, G.G., Tikhonov, A.N., Suzuki, N. (Eds.), The Yukagir Mammoth. Institute of Applied Ecology of the North [Yakutsk], St. Petersburg, pp. 97–118.

Moss, C.J., 1988. Elephant Memories: Thirteen Years in the Life of an Elephant Family. William Morrow, New York.

Nicholson, W.L., Krivushin, K., Gilichinsky, D., Schuerger, A.C., 2013. Growth of *Carnobacterium* spp. from permafrost under low pressure, temperature, and anoxic atmosphere has implications for Earth microbes on Mars. Proc. Natl. Acad. Sci. U. S. 110 (2), 666–671. http://dx.doi.org/10.1073/pnas.1209793110.

O'Sullivan, L., Ross, R.P., Hill, C., 2002. Potential of bacteriocin-producing lactic acid bacteria for improvements in food safety and quality. Biochimie 84, 593–604.

Papageorgopoulou, C., Link, K., Rühli, F.J., 2015. Histology of a woolly mammoth (*Mammuthus primigenius*) preserved in permafrost, Yamal Peninsula, northwest Siberia. Anatomical Rec. 298, 1059–1071.

Pitulko, V.V., Tikhonov, A.N., Pavlova, E.Y., Nikolskiy, P.A., Kuper, K.E., Polozov, R.N., 2016. Early human presence in the Arctic: evidence from 45,000-year-old mammoth remains. Science 351 (6270), 260–263.

Roth, V.L., Shoshani, J., 1988. Dental identification and age determination in *Elephas maximus*. Journal of Zoology, London 214, pp. 567–588.

Rountrey, A.N., 2009. Life Histories of Juvenile Woolly Mammoths from Siberia: Stable Isotope and Elemental Analyses of Tooth Dentin. University of Michigan, USA. Ph.D. dissertation.

Rountrey, A.N., Fisher, D.C., Vartanyan, S., Fox, D.L., 2007. Carbon and nitrogen isotope analyses of a juvenile woolly mammoth tusk: evidence of weaning. Quat. Int. 169–170, 166–173.

Rountrey, A.N., Fisher, D.C., Tikhonov, A.N., Kosintsev, P.A., Lazarev, P.A., Boeskorov, G., Buigues, B., 2012. Early tooth development, gestation, and season of birth in mammoths. Quat. Int. 255, 196–205.

Shilo, N.A., Lozhkin, A.V., Titov, E.E., Shumilov, Y.V., 1983. Kirgilyakh Mammoth (Paleogeographical Aspect). Nauka, Moscow (In Russian).

Smith, K.M., Fisher, D.C., 2011. Sexual dimorphism of structures showing indeterminate growth: tusks of American mastodons (*Mammut americanum*). Paleobiology 37 (2), 175–194.

Smith, K.M., Fisher, D.C., 2013. Sexual dimorphism in inter-generic variation in proboscidean tusks: multivariate assessment of American mastodons (*Mammut americanum*) and extant African elephants. J. Mammalian Evol. 20, 337–355.

Sukumar, R., Joshi, N.V., Krishnamurthy, V., 1988. Growth in the Asian elephant. Proc. Indian Acad. Sci. (Animal Sci.) 97 (6), 561–571.

Szpak, P., Gröcke, D.R., Debruyne, R., MacPhee, R.D.E., Guthrie, R.D., Froese, D., Zazula, G.D., Patterson, W.P., Poinar, H.N., 2010. Regional differences in bone collagen $\delta^{13}C$ and $\delta^{15}N$ of Pleistocene mammoths: implications for paleoecology of the mammoth steppe. Palaeogeography, Palaeoclimatology, Palaeoecology 286, 88–96.